CMB heat flux: local negative patches and hints from seismic tomography

Frédéric Deschamps, Joshua Guerrero, Sheng-An Shih, Hagay Amit, Gaël Choblet

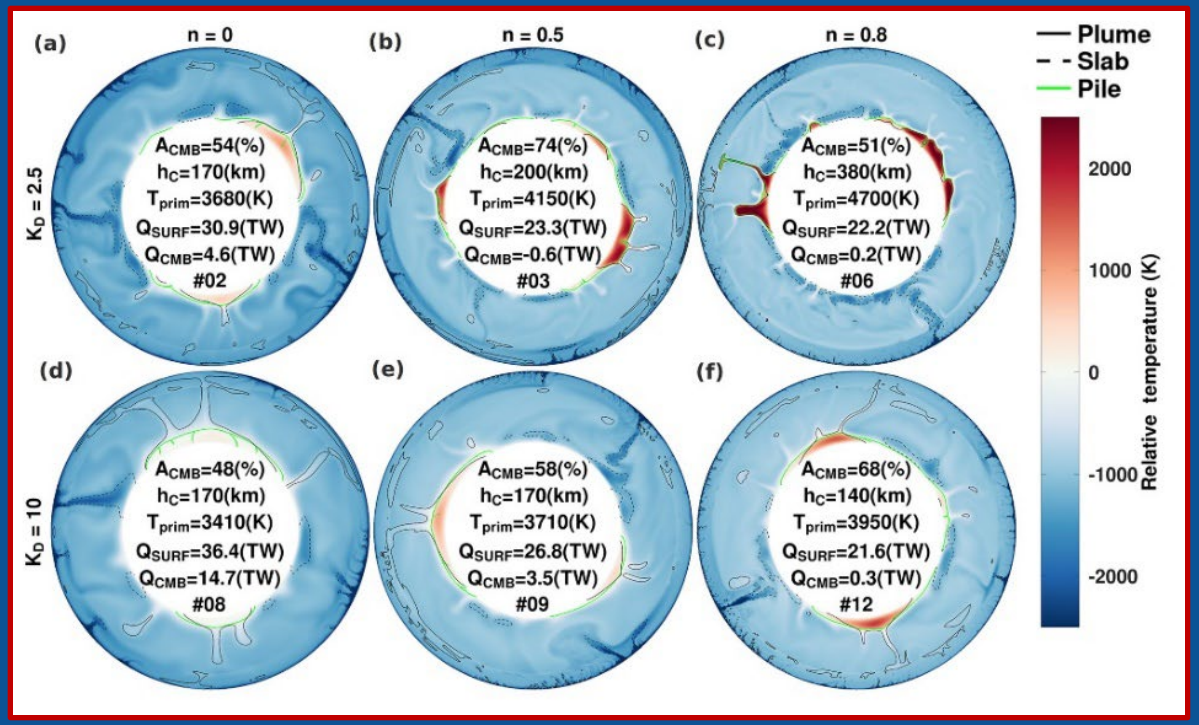

DYRE-COMB meeting – July, 8th 2025

Motivations

▸ Heat flux at core-mantle boundary (CMB), Φ_{CMB} = kdT/dr, and its variations (spatial and temporal) impact core dynamics.

▸ Seismic tomography: strong variations in shear wave velocity at the bottom of the mantle, suggesting lateral changes in chemistry and temperature, and thus in heat flux.

LLSVPs : hotter and chemically differentiated regions beneath Africa and the Pacific.

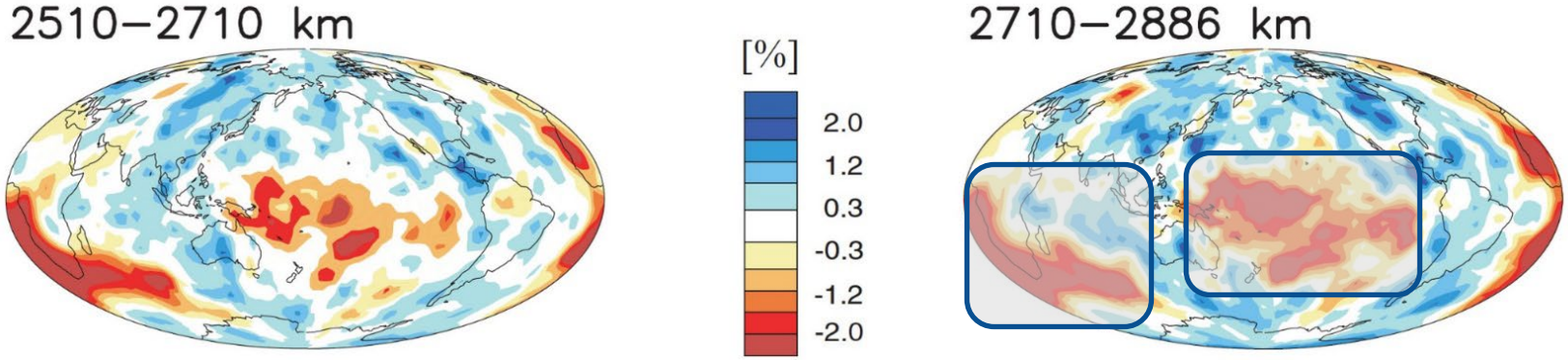

HMSL-S, *Houser et al. (2008)*

▸ No direct measurements of CMB heat flux. Need to access temperature gradient and its spatial variations.

▸ Temperature changes may be inferred from seismic tomography, but seismic velocity anomalies are unlikely purely thermal in origin.

Constraints from simulations of mantle convection

▸ Model CMB heat flux with simulations of thermo-chemical convection.

- Amplitude in heat flux variations.

- Heat flux beneath piles of dense material (modeling LLSVPs).

- Spatial and temporal variations depending on input parameters (e.g., temperature-dependent thermal conductivity, excess heating in piles).

▸ Mapping CMB heat flux from thermo-chemical structure deduced from simulations of mantle convection.

- Simulations of convection predict temperature, phase (post-perovskite), and compositional fields.

- Calculate synthetic velocity anomalies ($d\ln V_S$) and heat flux (Q_{CMB}) from these fields.

- Infer relationship between synthetic $d\ln V_S$ and Q_{CMB}.

Spatial and temporal variations

- Patches of negative heat flux may locally appear within piles of dense material located at the bottom of (Guerrero et al., *Solid Earth*, 2023).

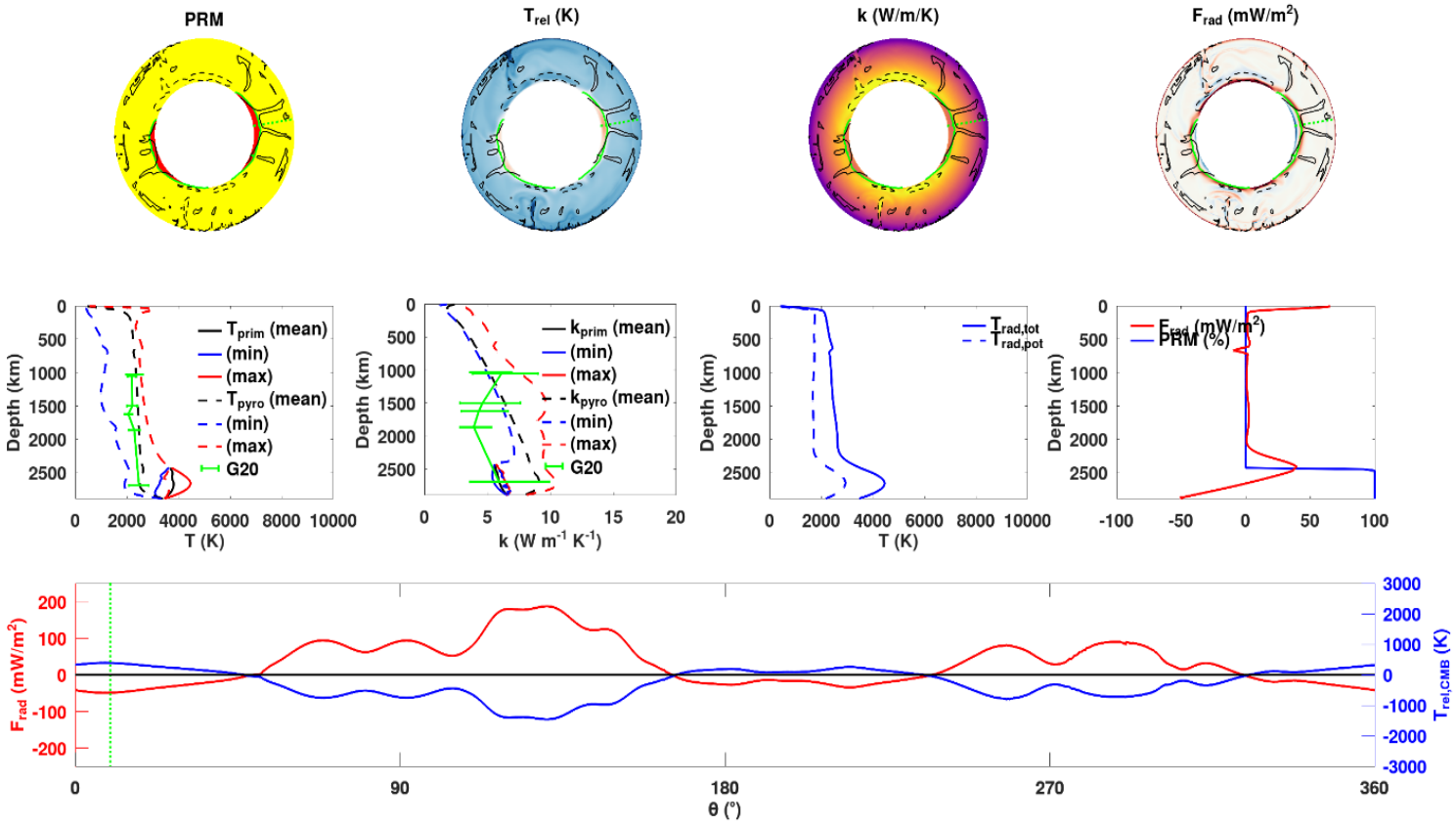

- Here, we investigate the conditions needed for generating such patches of negative heat flux, using simulations of thermo-chemical convection with StagYY.

Modeling and setup

- Simulation of thermo-chemical convection with StagYY (Tackley, 2014):

- Spherical annulus geometry with core/total radii ratio f = 0.55.

- Grid resolution : 2048×256 points, with refinement at top and bottom.

- Composition : volume fraction of dense material is set to x_{prim} = 4.0 % and buoyancy ratio to B = 0.23 (corresponding to density excess ~ 140 kg/m^3). Dense material, is initially distributed in a basal layer.

- Viscosity depends on temperature, pressure (with an additional viscosity ratio $\Delta\eta$ = 30 at 660 km) and composition. Yield stress (σ_Y) is imposed to avoid formation of a stagnant lid :

$$\eta = \frac{\eta_b \eta_Y}{(\eta_b + \eta_Y)} \quad \text{with}$$

$$\text{and} \quad \eta_b(z,T,C) = \eta_0 \left[1 + 29H(z-660)\right] \exp\left[V_a \frac{z}{D} + E_a \frac{\Delta T_S}{(T+T_{\text{off}})} + K_a C\right]$$

with E_a = 16.118 (corresponding to viscosity ratio of 10^7) from top to surface temperature, V_a = 2.303 (top-to-bottom viscosity ratio of 10), and K_a = 30 (dense material is 30 times more viscous than regular material).

- Internal heating rate R_H: dense material is assumed to have excess heating compared to regular material, controlled with ratio dH_{prim}. R_H is then given by :

$$R_H = \frac{H_{mantle}}{\left[1 + x_{prim}(dH_{prim} - 1)\right]}$$

In practice, R_H is chosen such that the total heating, H_{mantle}, is equal to 11 TW, consistent with Earth energy budget estimates (Jaupart et al., 2015) and corresponding to a heat flux of 21.6 mW/m^2 at the surface.

Modeling thermal conductivity

- Thermal conductivity depends on depth (pressure), temperature and composition as in Guerrero et al., *Solid Earth* (2023) and *EPSL* (2024):

- Depth dependence : follows mineral physics data for olivine (UM ; Chang et al., 2017) and bridgmanite and ferro-periclase (LM ; Hsieh et al., 2017, 2018). This is equivalent to an intrinsic top-to-bottom increase of ~ 27 (at 300 K and excluding adiabatic effect), and ~ 9 along a 2000 K adiabat.

- Temperature dependence : conductivity decreases with increasing temperature as $1/T^a$. We explored values of a in the range $0.0 < a < 1.0$.

For lower mantle minerals, experimental data suggest a in the range 0.2-0.4.

- Compositional dependence : dense material conductivity is assumed to be 20 % lower than regular material conductivity. This accounts for the presence of material enriched in iron by ~ 4 % in LLSVPs (Deschamps and Hsieh, GJI, 2019).

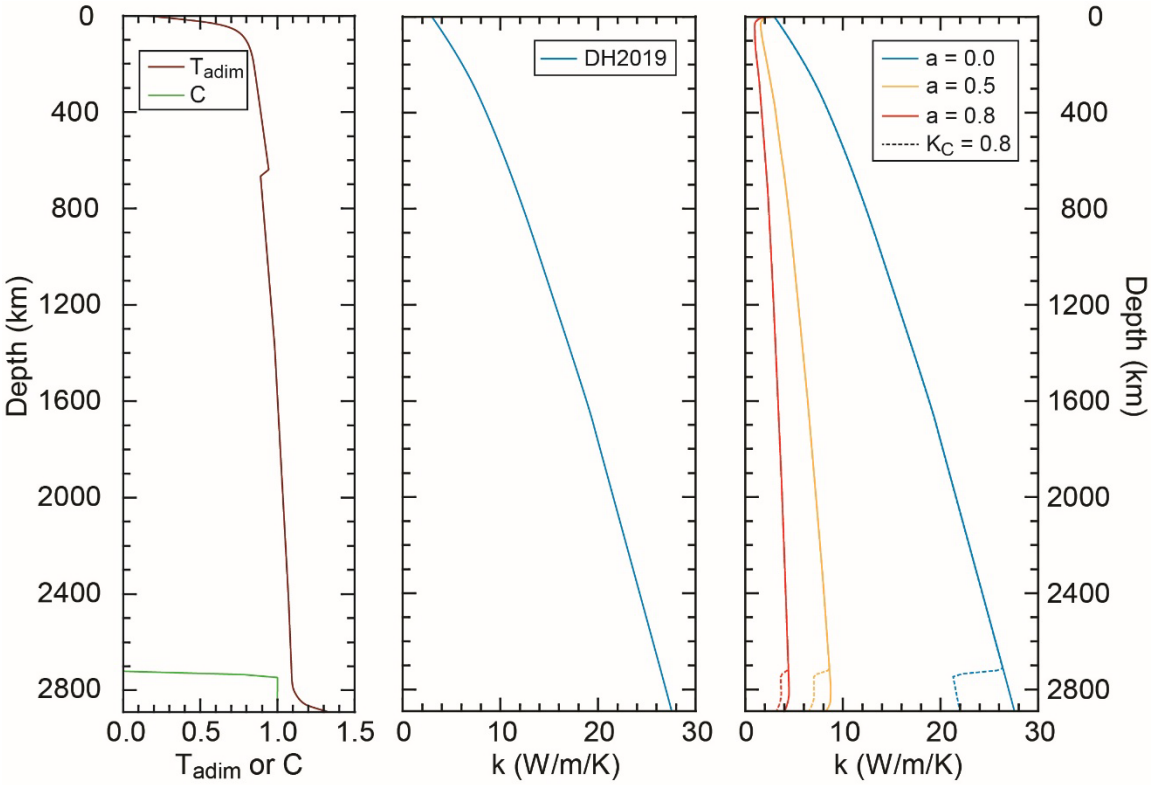

Simulations of thermo-chemical convection

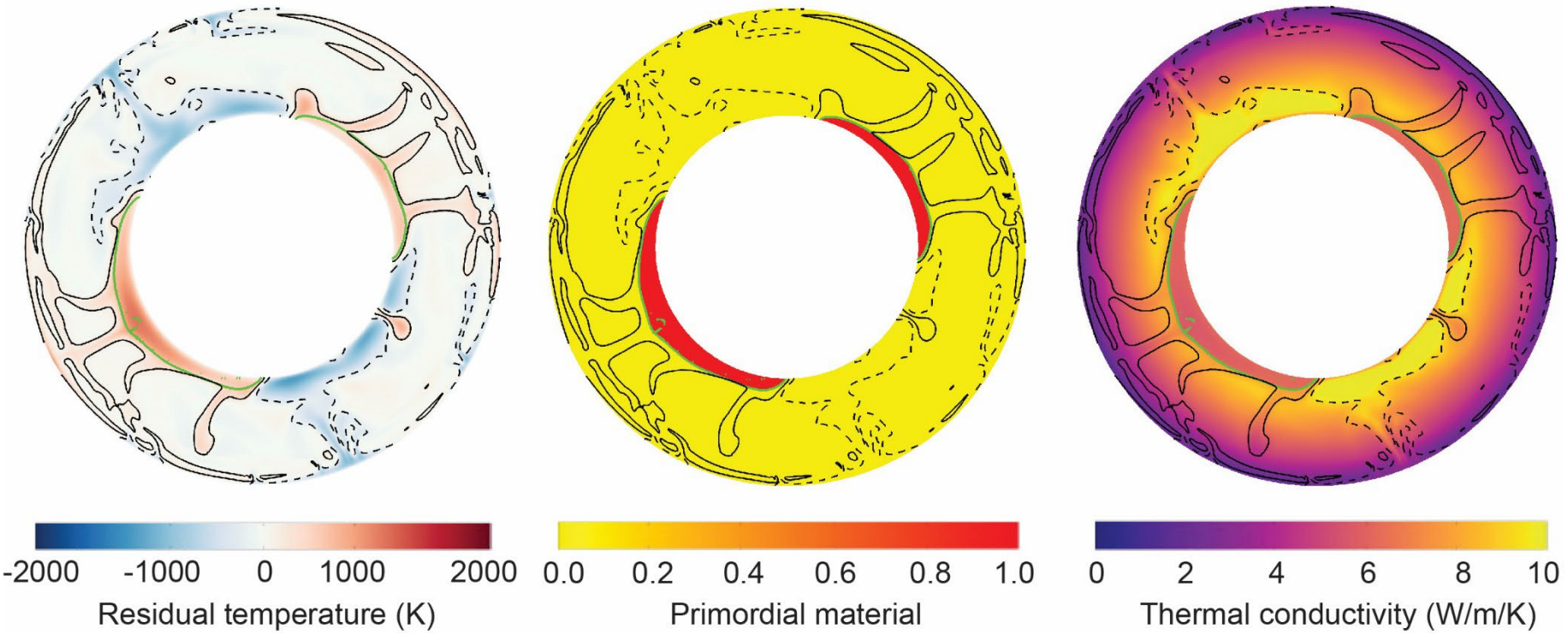

$R_H = 10$; $k \sim 1/T^{0.5}$

- Formation of hot piles of dense material at the CMB.
- Plumes are being generated at the top of these piles.
- Piles are thermally less conductive than surrounding mantle.

Varying a and dH_{prim}: temperature fields

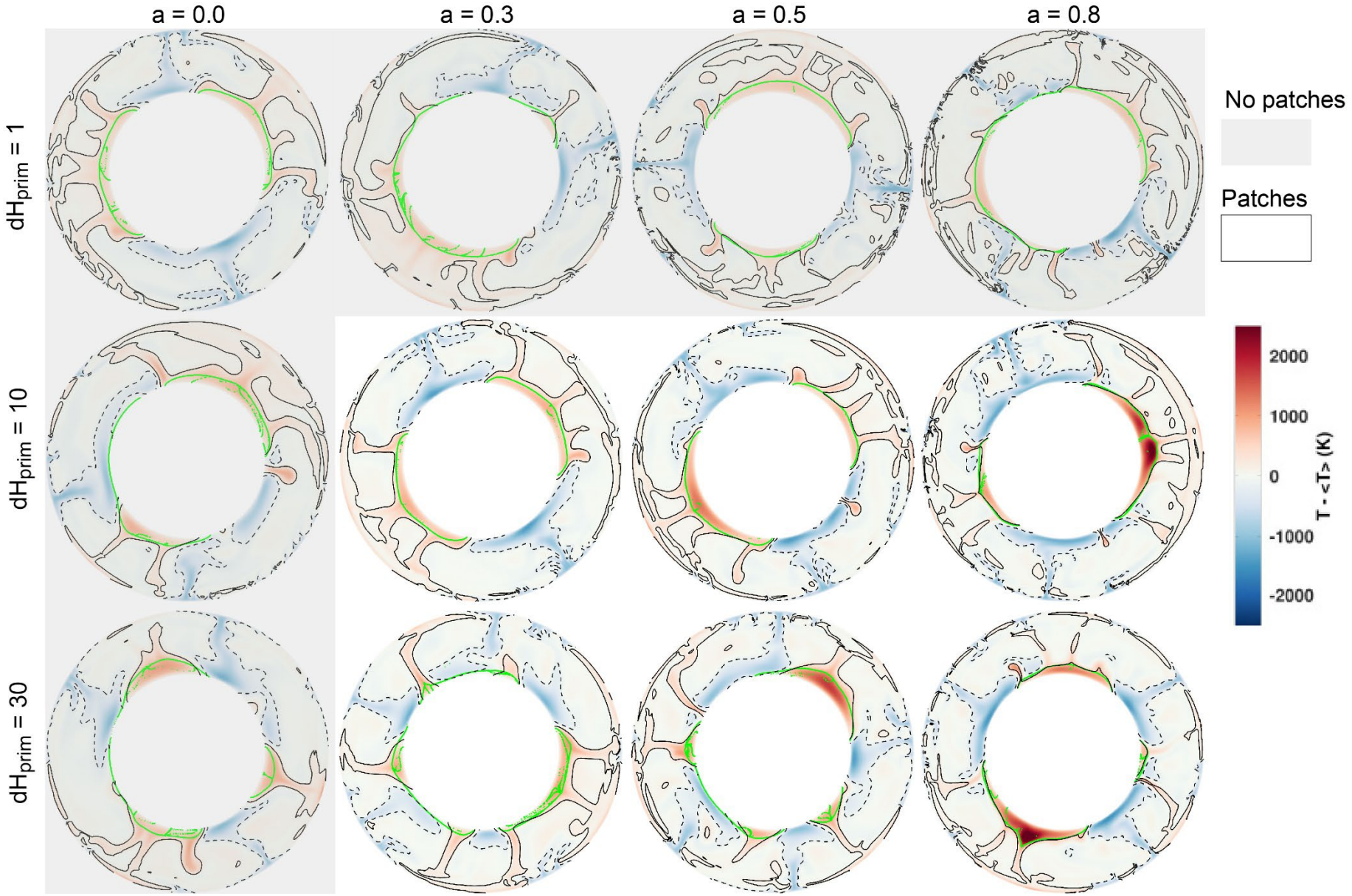

Conditions for generating patches of negative heat flux

- Negative heat flux patches appear for temperature exponent $a > 0.1$ and excess heating $dH_{prim} \geq 2$.
- Threshold value of dH_{prim} increases with decreasing temperature-dependence (lower a).
- For weak temperature dependence (low a), patches disappear again at high dH_{prim}.

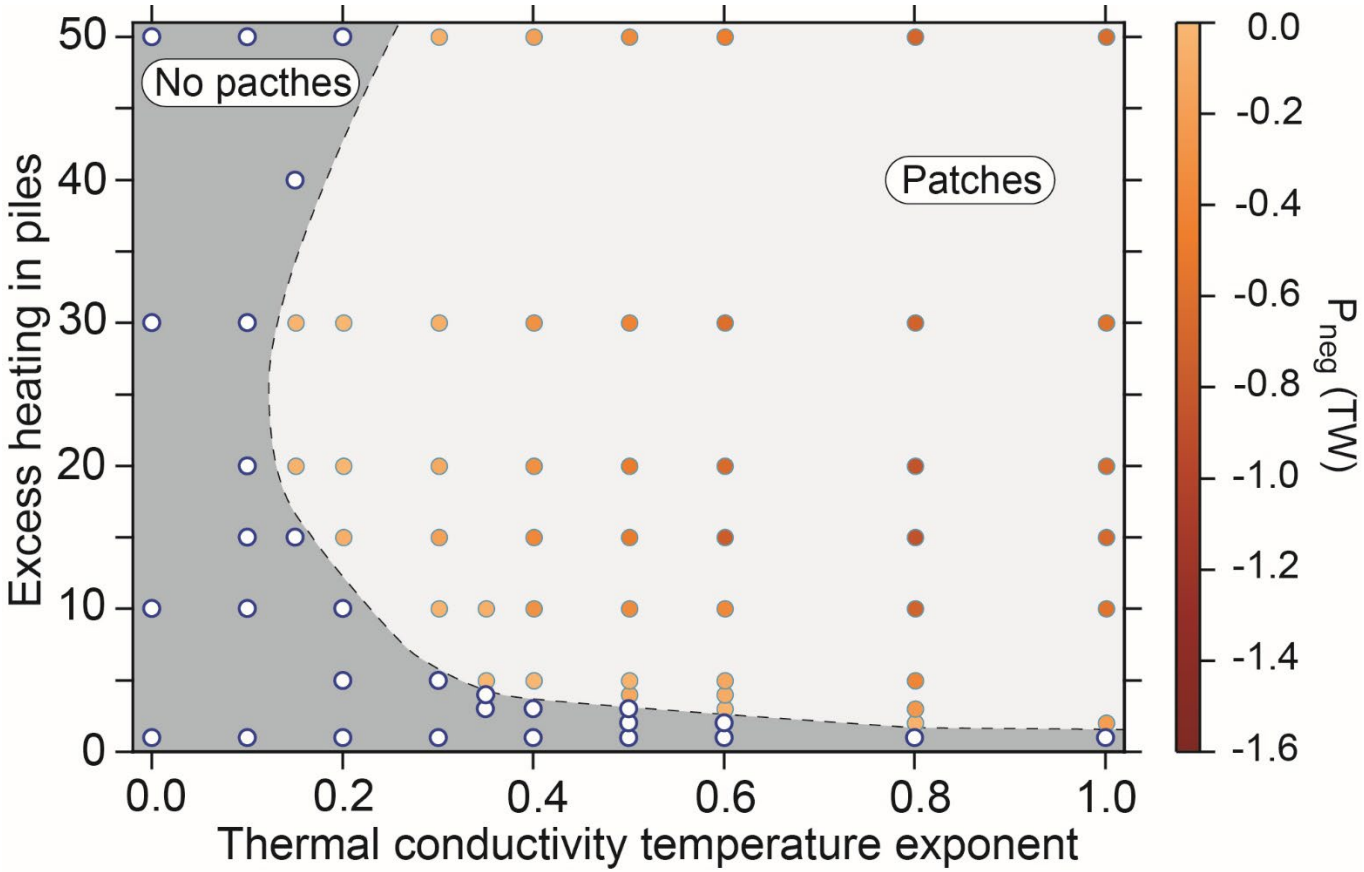

CMB heat flux variations and piles topography

- Patches of negative heat flux appear well within piles interiors (not at their edges), where topography is highest.

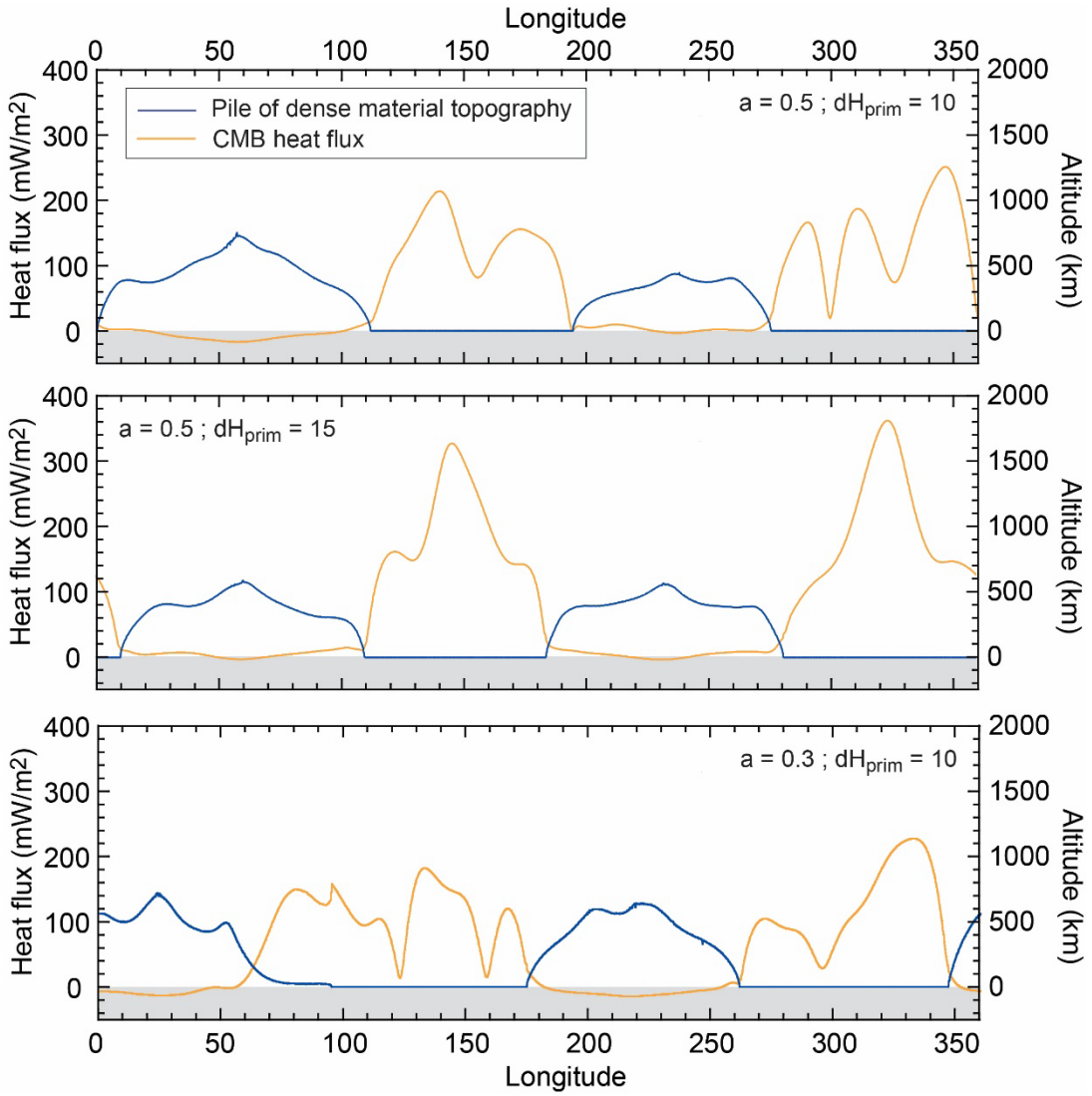

Power flowing to the core

- The power flowing to the core increases with *a.* It also increases with excess heating but only up to some given value of the (dH_{prim} ~ 15), and then starts decreasing again.

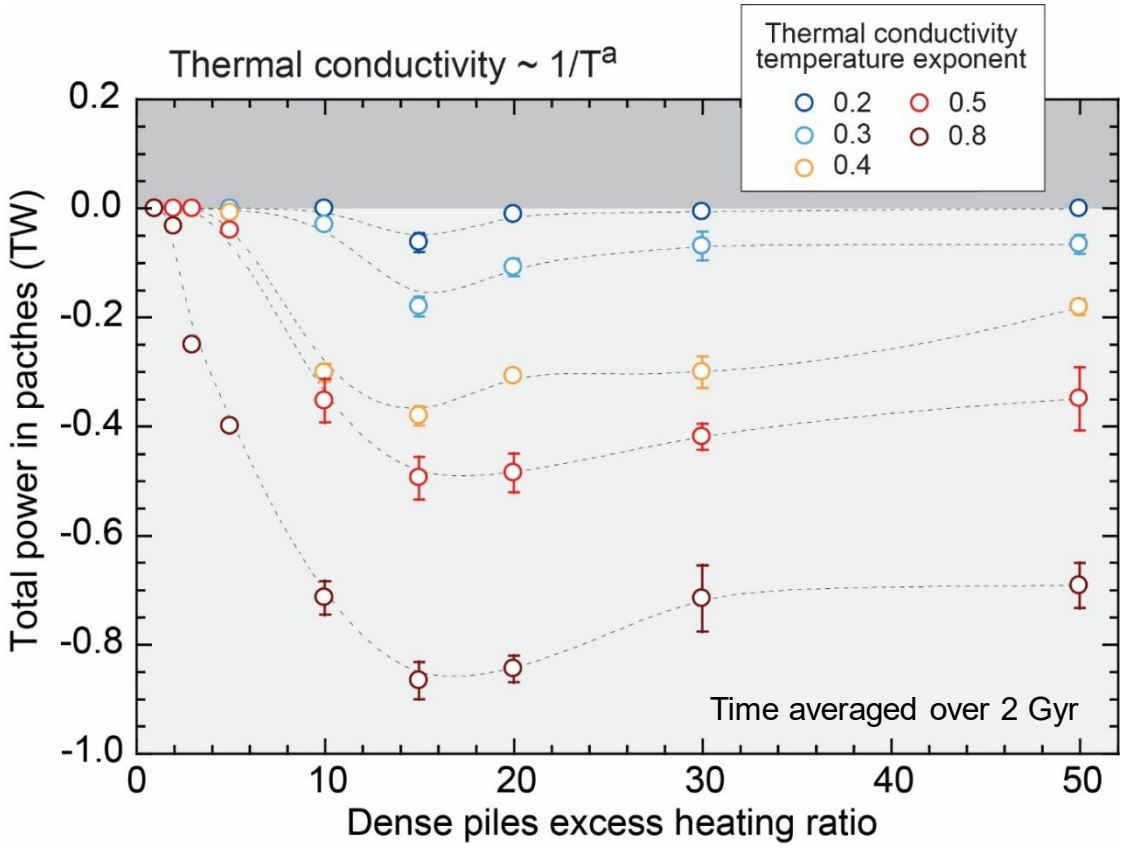

- Piles temperature increases with excess heating, but heating rate elsewhere in the mantle decreases.

As a result, plumes generated at the top of piles are stronger and extract more heat from piles.

Average CMB heat flux

- Average CMB heat flux (<*Q*>) decreases with increasing temperature-dependence of conductivity (increasing *a*), and overall independent of excess heating in piles.
- For $0.2 < a < 0.8$, <Q> is consistent with estimated CMB total power (5-17 TW).

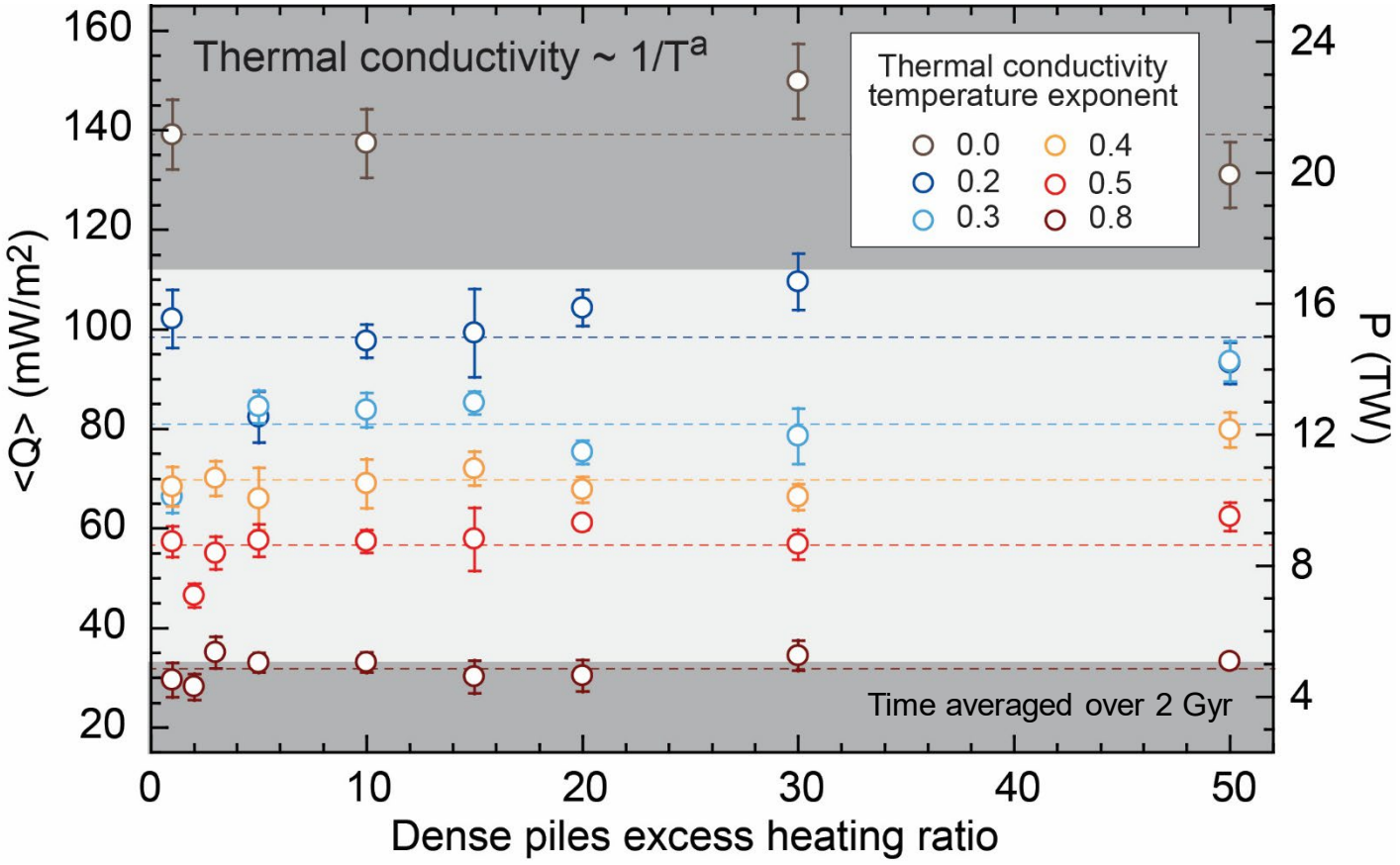

Consequence for core dynamics and evolution : q*

- Heat flux heterogeneity $q^* = \frac{(Q_{max} - Q_{min})}{2(Q_{avg} - Q_{adia}^{core})}$

Q_{adia}^{core} is set to 24 mW/m^2, assuming k_{core} = 40 W/m/K and $(dT/dz)_{adia}$ = 0.6 K/km

Higher q* favor magnetic field polarity reversals (*e.g.*, Terra-Nova and Amit, 2024).

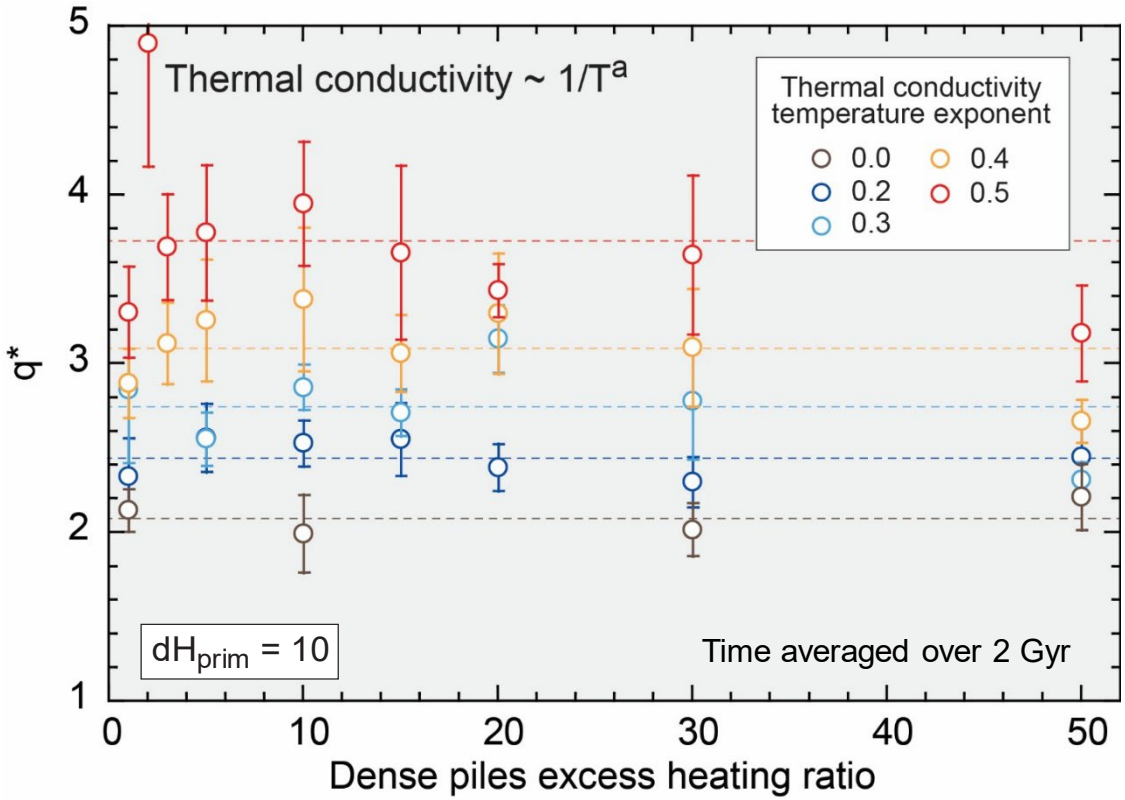

- Time-averaged q* increases with temperature dependence of conductivity (increasing *a*) : stronger temperature-dependence should promote magnetic reversals.

Time variations in q*

- Time variability of q* is important (> 0.5) and larger for higher temperature-dependence of conductivity (> 1 for *a* = 0.5).

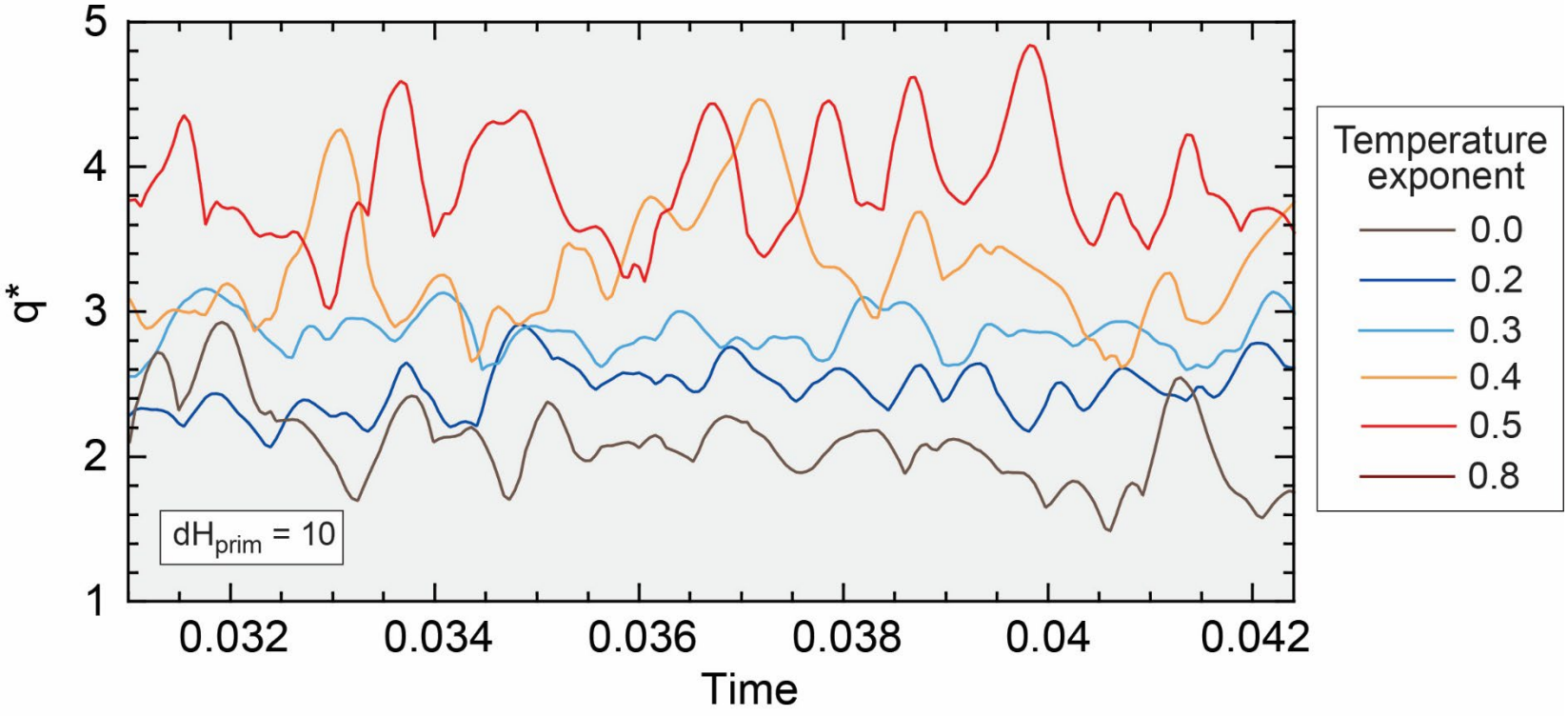

- May explain geomagnetic superchrones (low q* periods) and hyper-frequency reversals (high q* periods).

Patches of negative CMB heat flux

- Appearance:

- Need temperature-dependent thermal conductivity.

- Need excess internal heating in piles of dense material.

- Location:

- Appear in piles interior, not at their edges.

- Good correlation with piles' height.

- Strength:

- Total power in patches (flowing to the core) increases with sensitivity of conductivity to temperature.

- Total power reaches a maximum value for some value of excess heating.

- Consequence for core dynamics:

- q* value and temporal variability increase with sensitivity of conductivity to temperature.

- May play a role in the frequency of magnetic field polarity reversals.

Mapped CMB heat flux

- Mappings can be applied to available seismic tomography (e.g., Houser et al., 2008) to recover Earth's CMB heat flux.

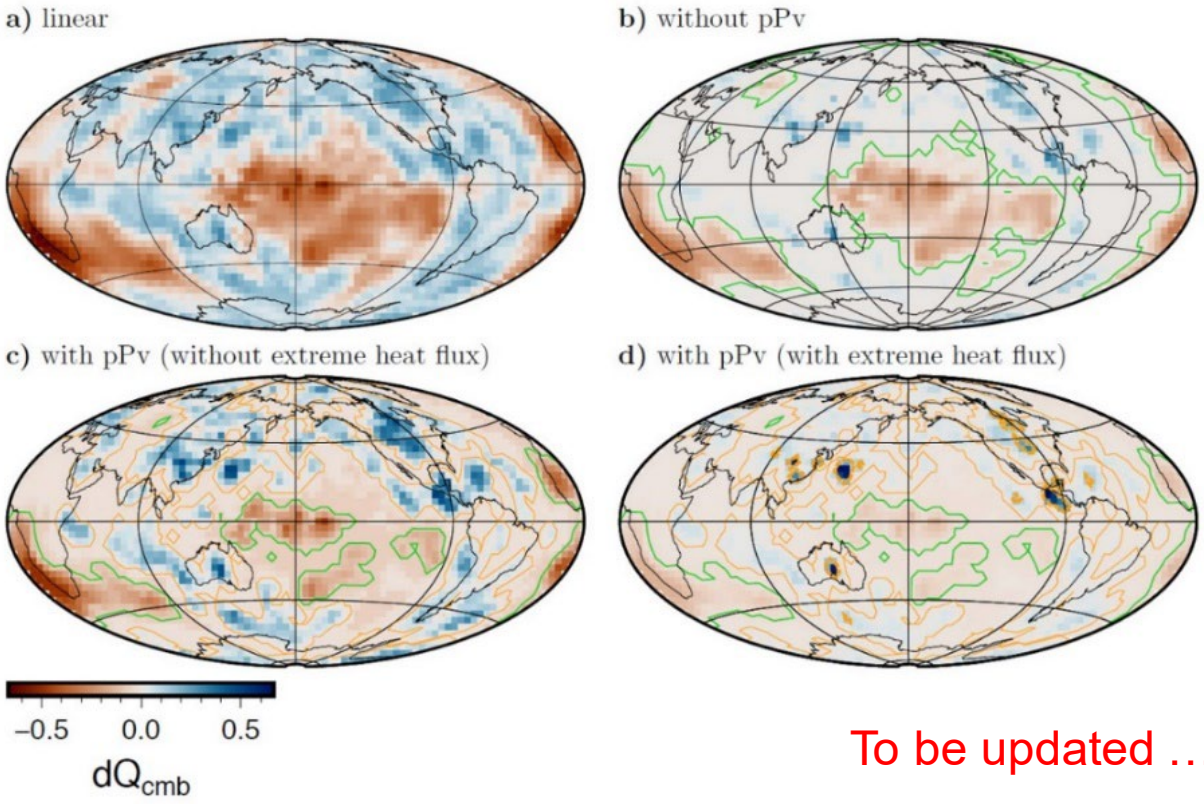

To be updated …

- Low heat flux anomalies beneath LLSVPs are attenuated, while large heat flux patches are enhanced.
- The presence of pPv further attenuates the low heat flux anomalies within LLSVPs

Dans les épisodes précédents …

Simulations of thermo-chemical convection

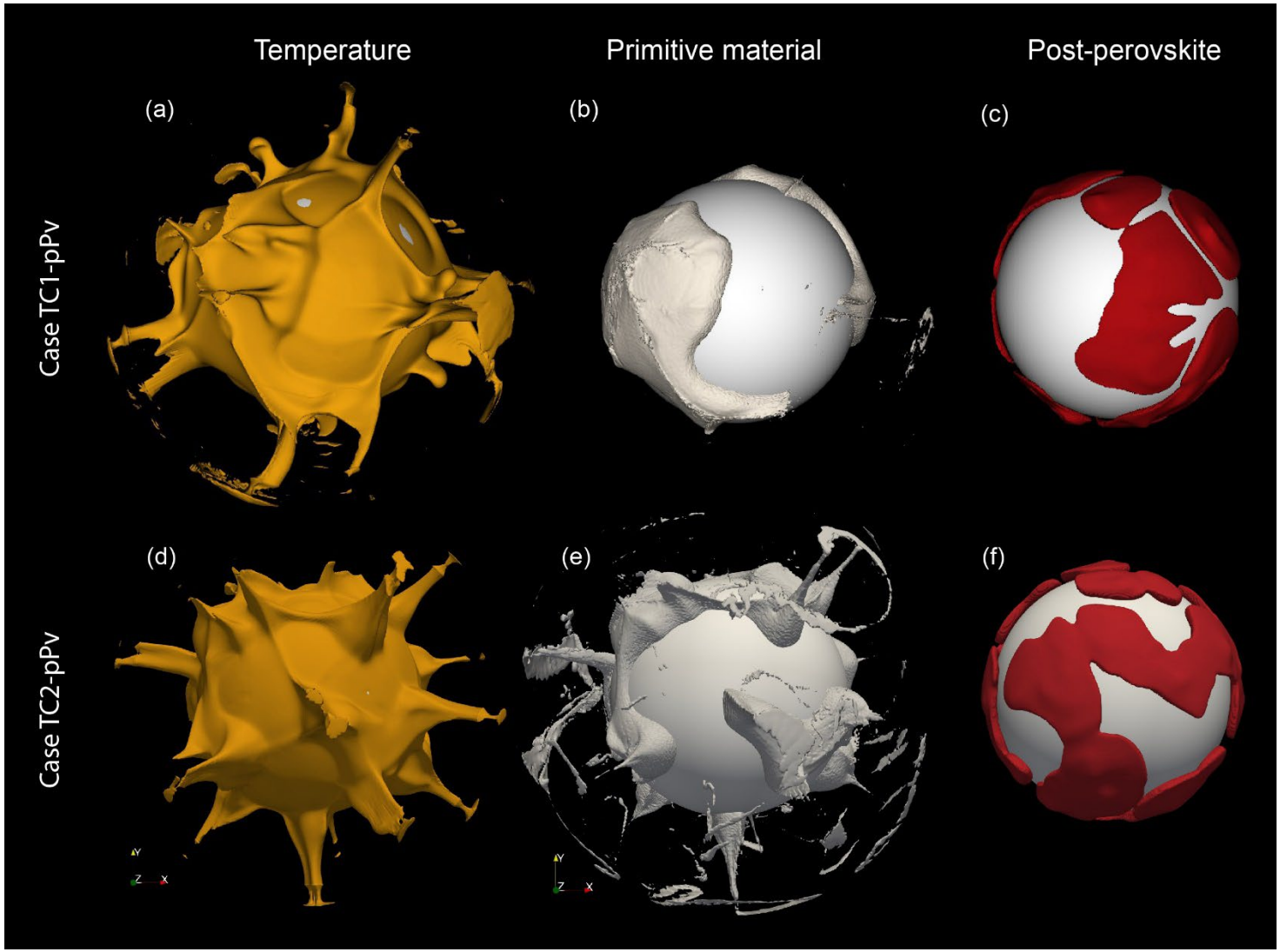

Mapping CMB heat flux from seismic velocities

- Simulations of thermo-chemical convection : temperature, phase (post-perovskite) and compositional fields.

- Calculate seismic shear velocity anomalies averaged in the bottom 200 km …

- ... and CMB heat flux (~ dT).

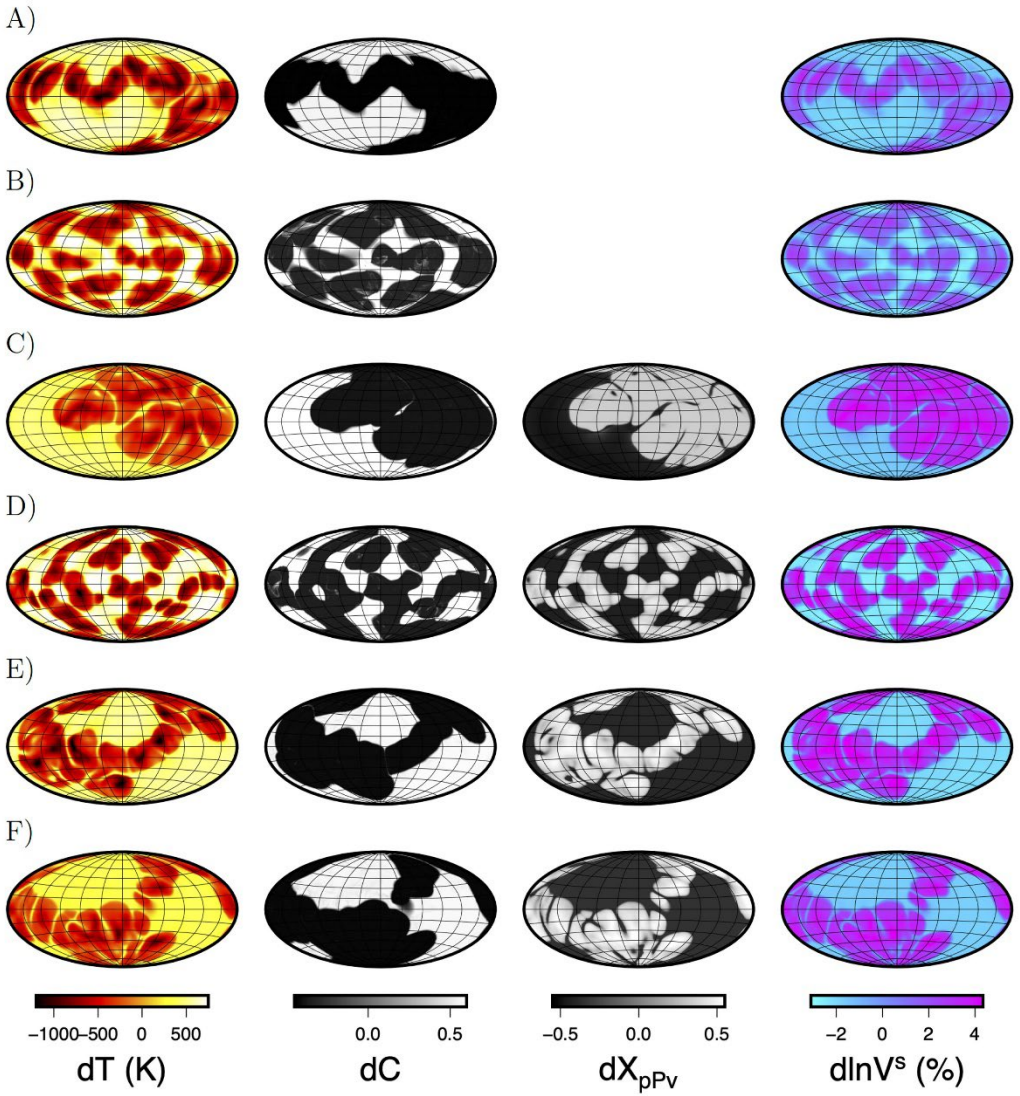

Choblet et al., submitted to PEPI

Mapping CMB heat flux from seismic velocities

- Determine synthetic relationships (mappings) between seismic velocities and heat flux.

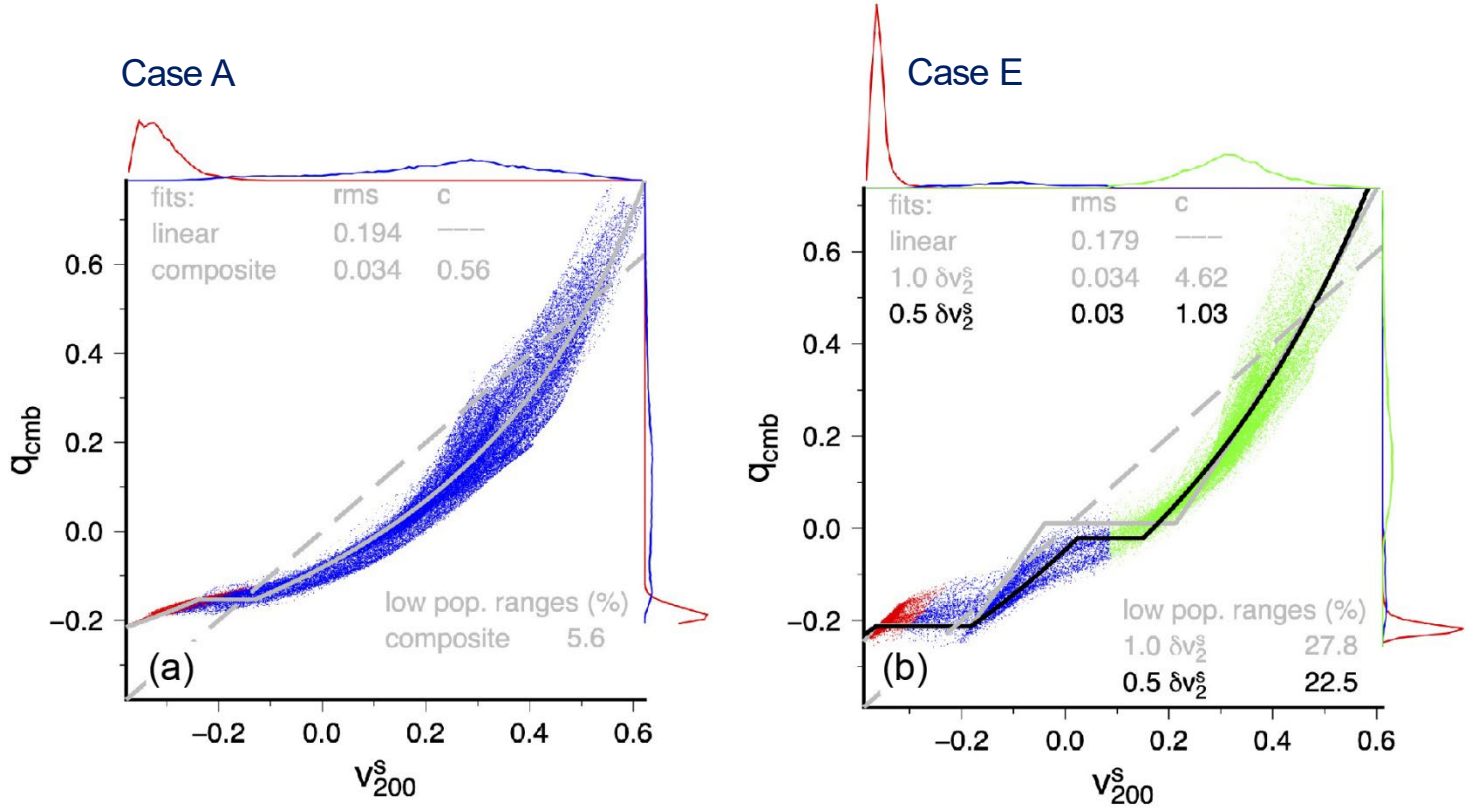

Choblet et al., PEPI, 2023

$$q = \frac{cv_T}{1 - v_T + c}$$

v_T : normalized thermal component of velocity anomaly.

Mapped CMB heat flux

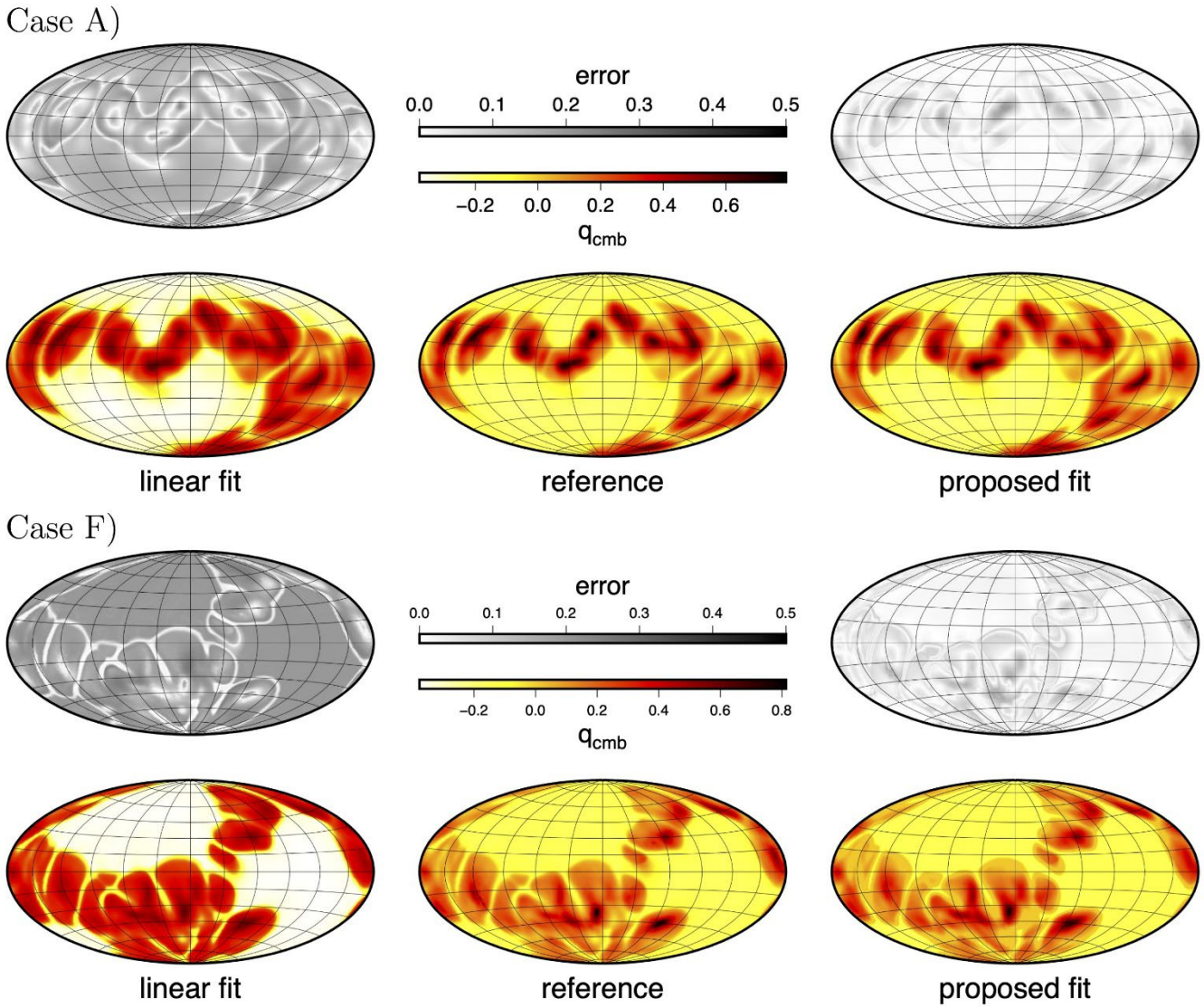

Tomographic models

GLAD-M35

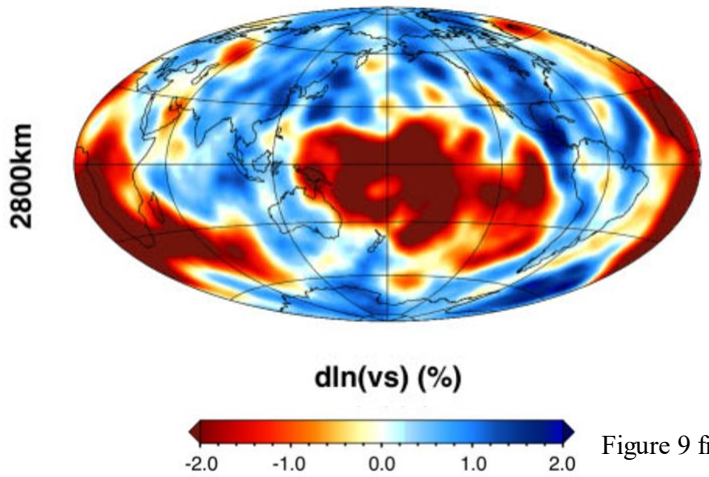

(max, min)=(2.75, -3.55)

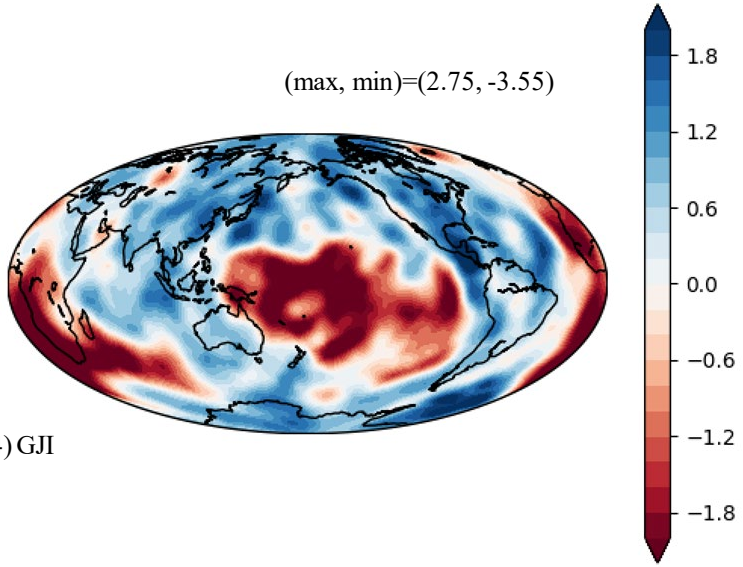

Figure 9 from Cui et al. (2024) GJI

SEMUCB-WM1

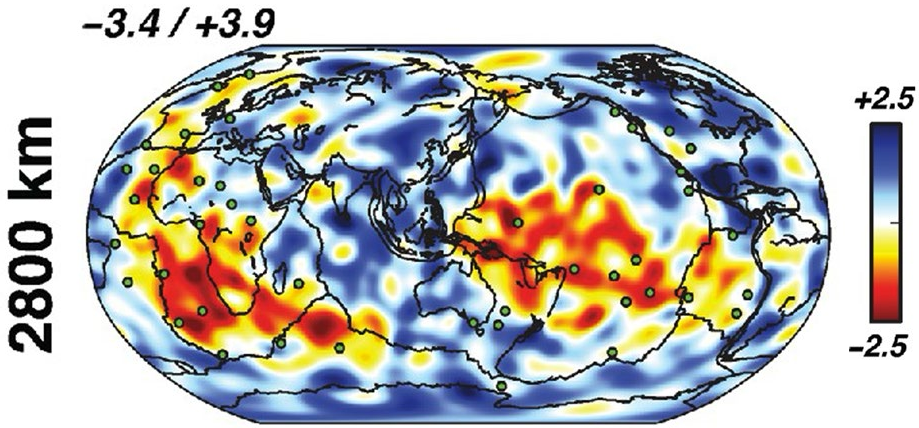

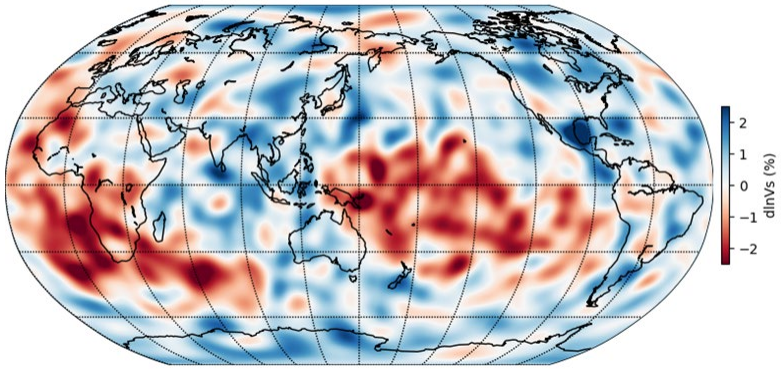

Figure 8 from French & Romanowicz (2014, GJI)

Finding 3 populations in Vs-tomography

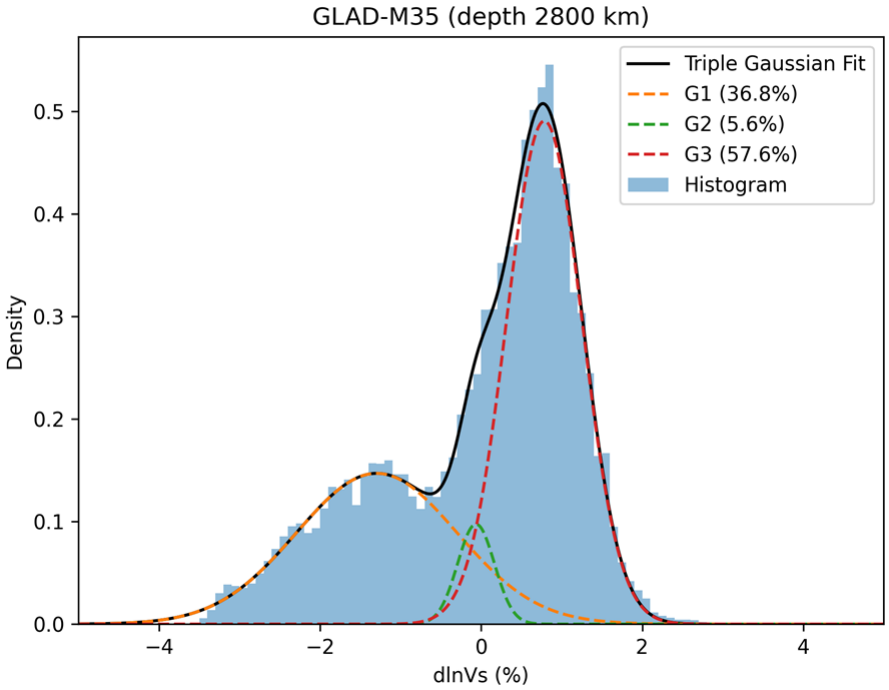

max, min = 2.75%, -3.55%
Fitted Gaussian parameters:
G1: amplitude = 0.15, mean = -1.30, std = 1.00
G2: amplitude = 0.10, mean = -0.06, std = 0.23
G3: amplitude = 0.49, mean = 0.78, std = 0.47

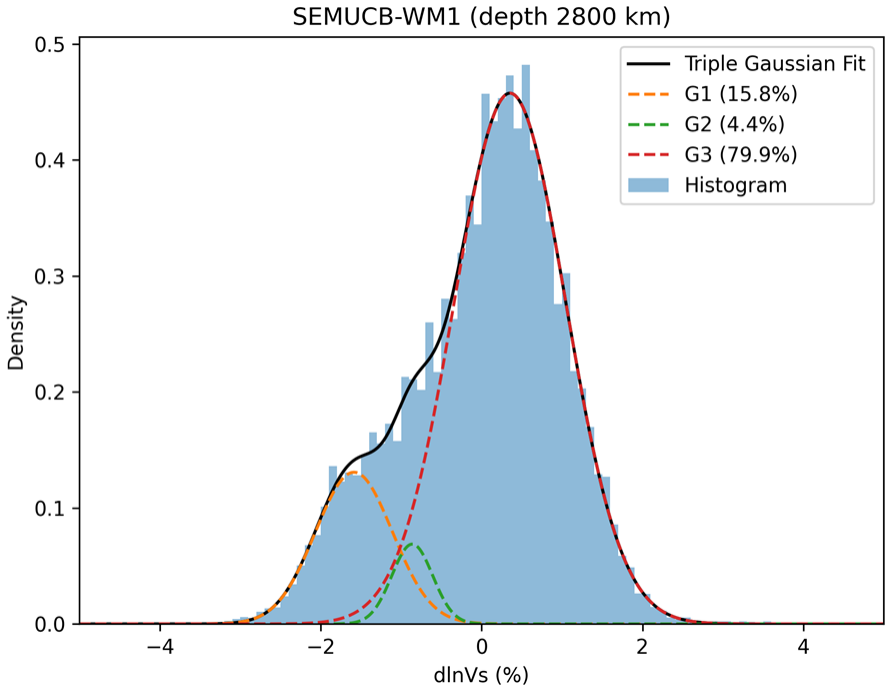

max, min = 3.73%, -3.63%
Fitted Gaussian parameters:
G1: amplitude = 0.13, mean = -1.59, std = 0.48
G2: amplitude = 0.07, mean = -0.86, std = 0.25
G3: amplitude = 0.46, mean = 0.35, std = 0.69

- Fit Vs frequency histograms with 3 Gaussian, representing 3 different populations.
- Boundaries between populations : set at fractions of standard deviations in each Gaussian.

Population distribution from GLAD-M35 (alternate)

- Population percentage calculated for each given dlnVs, using the fitted three Gaussian distributions.
- Vertical lines indicate the positions where any of the population percentages equals to 90%.
- Tails at high dlnVs in GLAD-M35 are due to the much slower decay rate of G1 compared to G3. This is an artifact of the method, that we should just ignore.

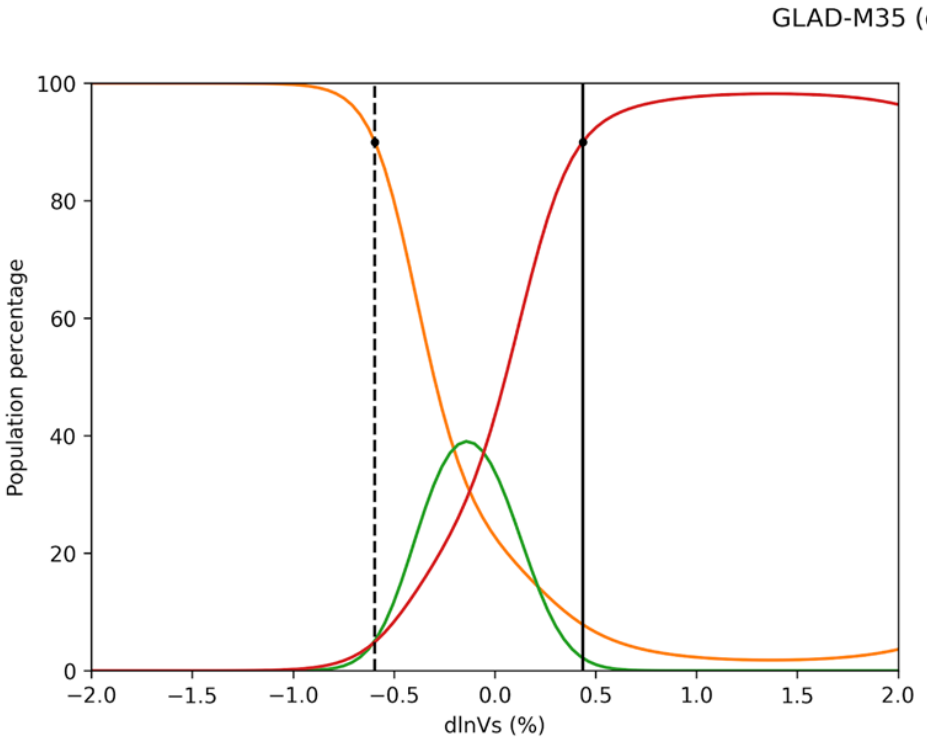

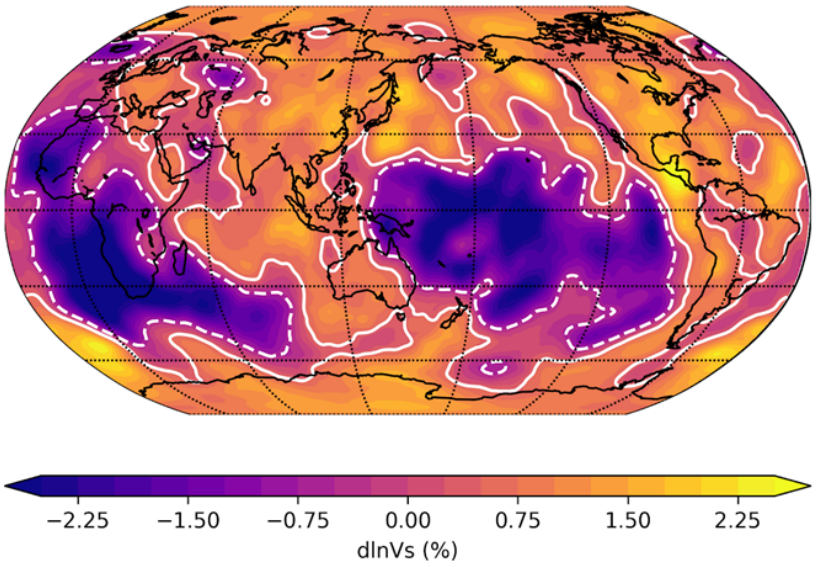

Population distribution from SEMUCB-WM1

- Population percentage calculated for each given dlnVs, using the fitted three Gaussian distributions.
- Vertical lines indicate the positions where any of the population percentages equals to 90%.

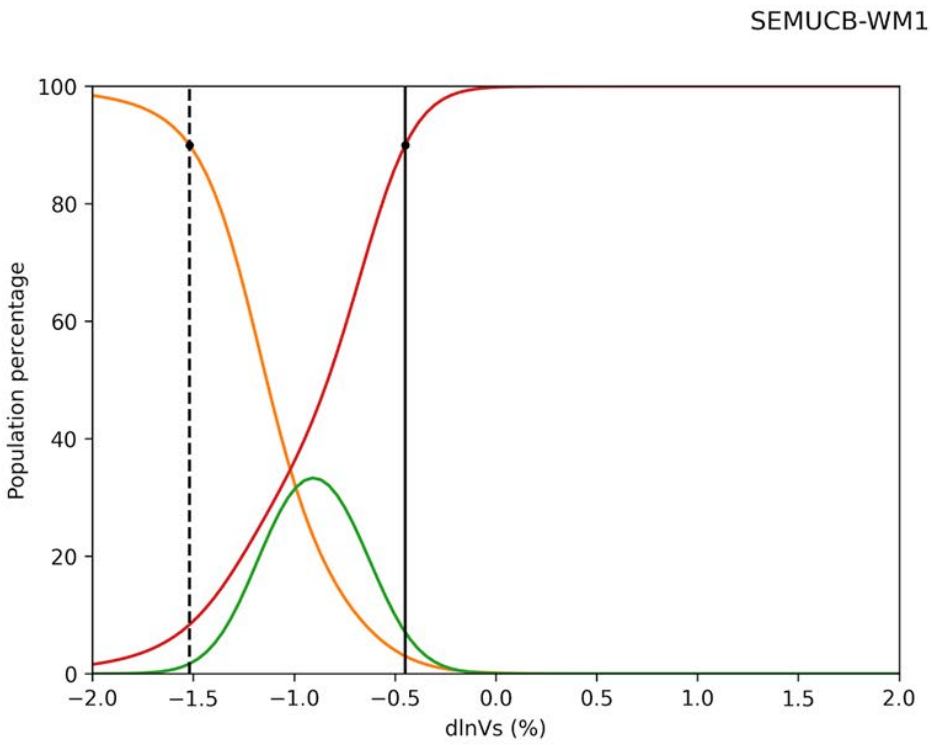

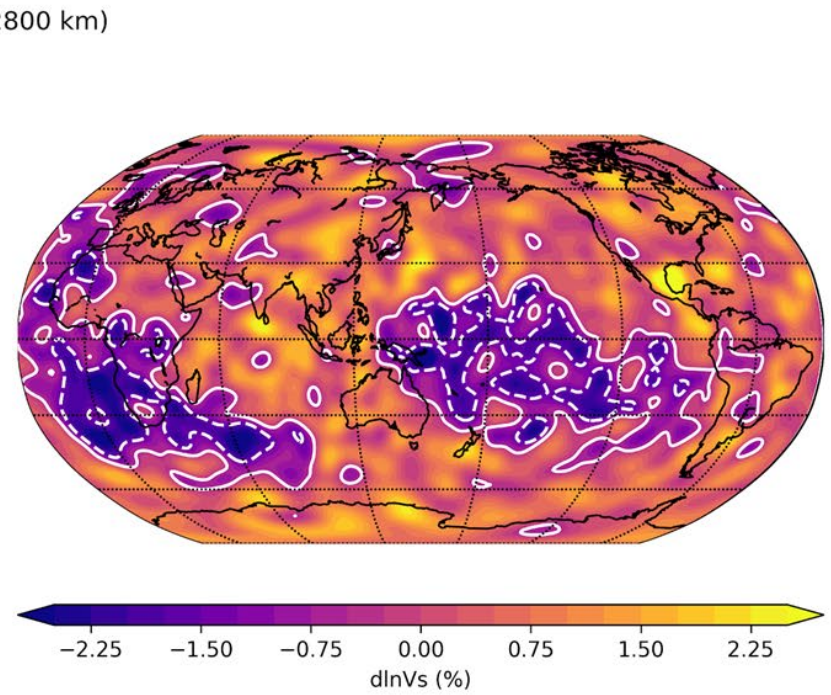

CMB heat flux from GLAD-M35

- Max/min (red dashed lines) are from dlnVs. Boundaries of delimiters are defined as 0.8 standard deviation from the mean of each group.

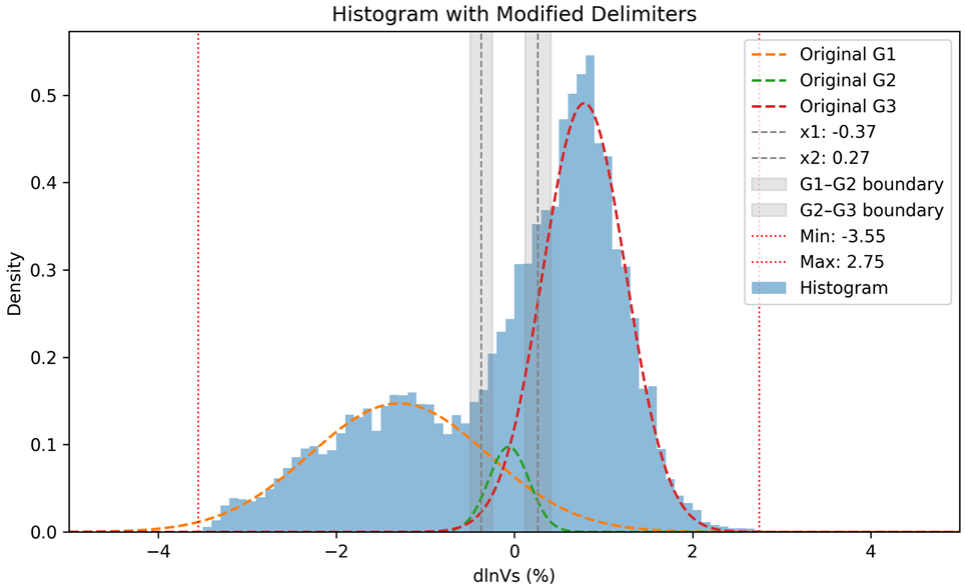

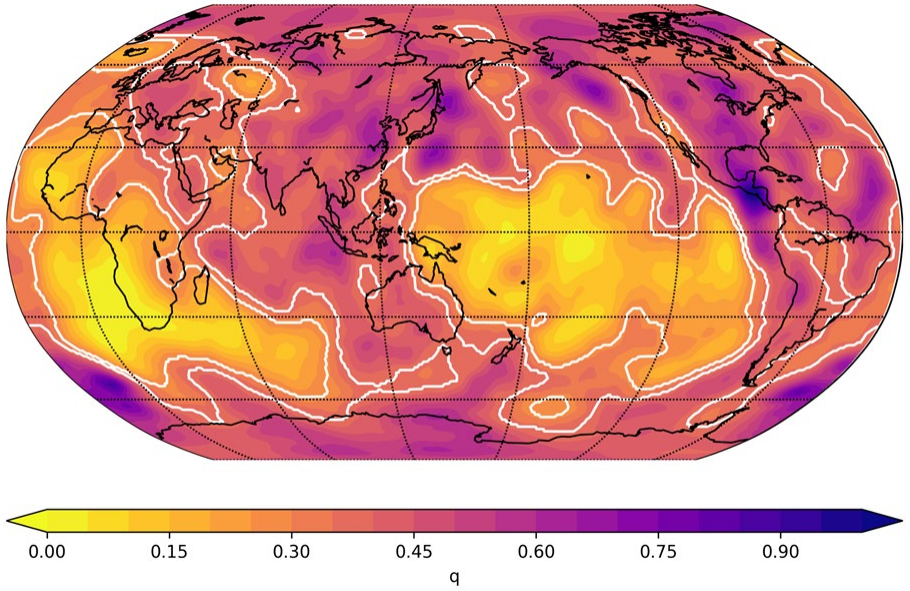

GLAD-M35

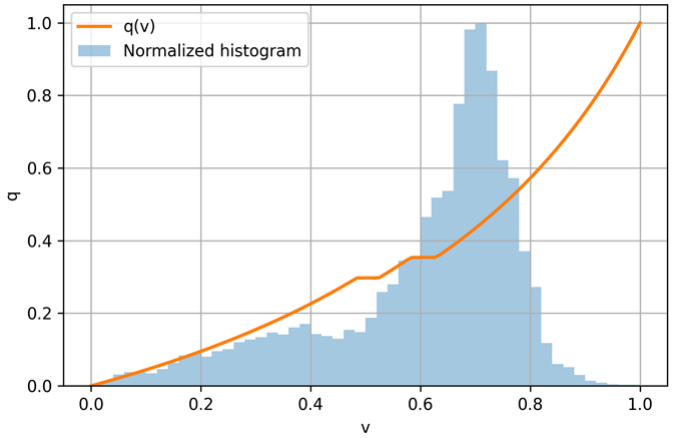

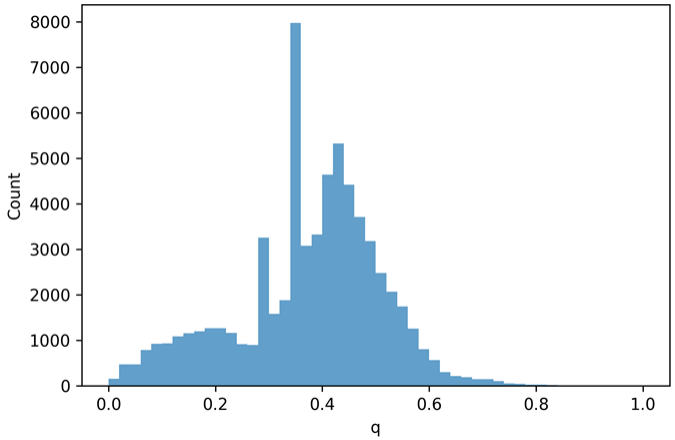

CMB heat flux from SEMUCB-WM1

- Max/min (red dashed lines) are from dlnVs. Boundaries of delimiters are defined as 0.8 standard deviation from the mean of each group.

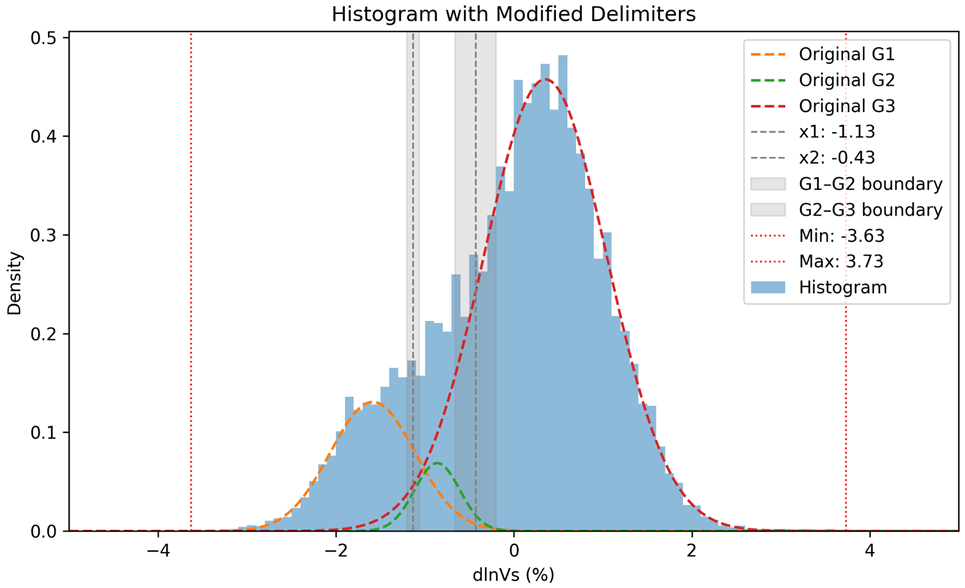

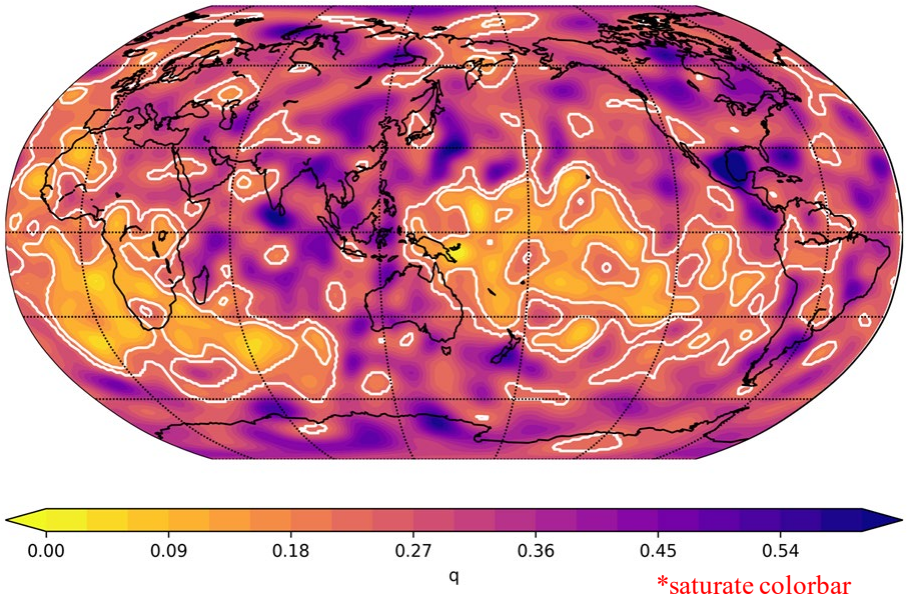

*saturate colorbar

SEMUCB-WM1

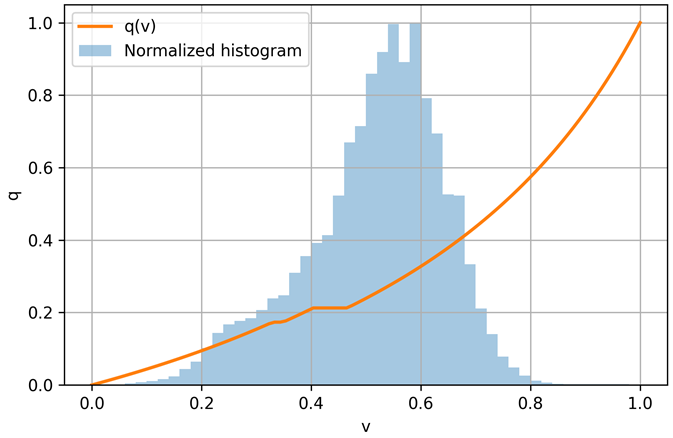

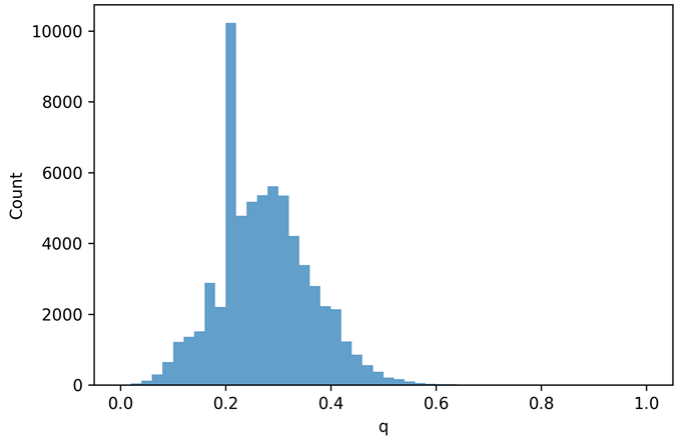

Mapping CMB heat flux

- Still in progress, but encouraging:

- Can distinguish 3 populations from shear-velocity frequency histograms.

- Conversion to heat flux: saturation issue. Should we use original Q-Vs parameterization or modify it ?